Exploring the mechanisms of the soil moisture-air temperature hypersensitive coupling regime

Hsin Hsu[1,2] (hh9736@princeton.edu), Paul A. Dirmeyer[2,3] and Eunkyo Seo[3,4]

[1]Princeton University, Princeton, NJ, USA

[2]George Mason University, Fairfax, VA, USA

[3]Center for Ocean-Land-Atmosphere Studies, George Mason University, Fairfax, VA, USA

[4]Department of Environmental Atmospheric Sciences, Pukyong National University, Busan, Republic of Korea

Key points:

- Hypersensitive regime acts throughout the chain of energy processes from land to atmosphere
- Hypersensitive regime occurs when soil moisture dries to the permanent wilting point
- Model's representation of evapotranspiration fundamentally governs the occurrence of hypersensitive regimes.

Abstract

High temperature extremes accompanied by drought have led to serious ramifications for environmental and socio-economic systems. Thus, improving the predictability of heat-wave events is a high priority. One key to achieving this is to better understand land-atmosphere interactions. Recent studies have documented a hypersensitive regime in the soil moisture-temperature relationship when soil dries below a critical low threshold, air temperatures increase at a greater rate as soil moisture declines. In this study, we explore the mechanisms linking low soil moisture to high air temperatures. From in-situ observations, we confirm that the hypersensitive regime acts throughout the chain of energy processes from land to atmosphere. A simple energy-balance model indicates that the cause of the hypersensitive regime is the dramatic drop in evaporative cooling that occurs when soil moisture dries to the permanent wilting point, below which latent heat flux almost ceases. Precisely how a model represents the relationship between evapotranspiration and soil moisture is found to be essential to describe the occurrence of hypersensitive regime. Thus, we advocate that climate models should ensure a realistic representation of land-atmosphere interactions to obtain reliable forecasts of extremes and climate projections, aiding the assessment of climate vulnerability and adaptation.

Plain-language summaries

Hot temperature extremes combined with droughts have caused significant problems for the environment and economies. Improving prediction of heat-wave events is of utmost importance. This can be achieved by a better understanding of how land conditions affect near surface atmosphere and vice versa. Recent evidences have shown that when the soil becomes very dry and below a certain threshold, even a slight decrease in soil moisture yields a substantial increase in air temperature. However, the behind mechanism remains unclear. In this study, we validate that hypersensitive regimes indeed result from energy transmission from land to atmosphere by using observations. Subsequently, we built a simple model to explore how air temperature correlates to land wetness conditions. Our model indicates that hypersensitive regime occurs when there is a dramatic drop in evaporation when soil moisture dries to the permanent wilting point, below which water is no longer drawn from the soil by plant roots. The diminished evaporation significantly curtails the cooling effect on the atmosphere. Notably, the model's representation of evaporation behavior fundamentally governs the occurrence of hypersensitive regimes. To achieve reliable forecasts of climate extremes and projections, a realistic depiction of land-atmosphere interactions is indispensable.

1. Introduction

Heatwaves have dramatic ramifications for socioeconomic, ecological, and hydrologic systems (Zaitchik 2006; Coumou and Rahmstorf, 2012; Zander et al. 2015). The increase in frequency and intensity of heatwaves and concomitant drought in recent decades calls for a better understanding of these extreme events (Perkins et al. 2012; Sheridan and Lee 2018; Founda et al. 2019; Yu et al. 2019). Such extremes are usually driven by atmospheric conditions — in most cases, there is tropospheric subsidence induced by a quasi-stationary high pressure system that suppresses the likelihood of precipitation, leading to unremitting hot and dry conditions near the surface (Della-Marta et al 2007; Alvarez-Castroet al 2015). Certain phases of natural variability in the atmosphere alter regional circulations (Sutton and Hodson 2005; Perkins-Kirkpatrick et al. 2017; Horton et al. 2015; Marotzke and Forster 2015), or recurrent patterns of stationary planetary waves (Petoukhov et al 2013; Kornhuber et al. 2017) that can be responsible for the occurrence of these abnormal synoptic conditions. Additionally, there are studies suggesting global warming can also be a significant contributor (Wehrli et al 2019; Seo et al. 2020). Nevertheless, it appears many regional drought/heat wave episodes cannot be fully explained without considering the contribution of land-atmosphere interactions, which can act to maintain or even exacerbate these abnormal hot and dry conditions (Seneviratne et al. 2006, 2010; Miralles et al 2014; Vogel et al. 2017; Schumacher et al. 2022, Mukherjee et al. 2023).

Normally, the incoming radiation energy at the land surface is partly consumed by land evaporation and vegetation transpiration that is released as latent heat flux (*LE*) (Santanello et ai. 2018). Anomalous dry soil conditions reduce *LE*, accompanied by enhanced sensible heat flux (*H*), which results in warming and drying of air near the surface (Eltahir 1998; Schwingshackl et al. 2017). As moisture sources such as precipitation are rare during heatwave/drought episodes, a feedback loop is established within which growing deficits in soil moisture content leads to even warmer air temperatures, aiding the persistence and bolstering the magnitude of heatwaves (Whan et al 2015; Vogel et al 2018; Erdenebat and Sato 2018; Seo et al. 2019). In addition to local land surface processes, amplification of heatwaves can be induced by upwind dry land conditions, where the resulting hot air is advected to downwind regions exacerbating extreme temperatures (Schumacher et al. 2019). The prerequisites of the phenomena mentioned above are that soil moisture variations in the moisture-limited regime, when available energy is plentiful, lets *LE* be sensitive to soil moisture variations. In contrast, in an energy-limited regime, the amount of *LE* is controlled by available energy instead of soil moisture (Seneviratne et al. 2010; Budyko 1974; Koster and Milly 1997; Zeppetello et al 2019; Hsu and Dirmeyer 2022).

Recent analysis with in-situ observations of land and near-surface atmospheric variables over North America (Benson and Dirmeyer 2021) and Europe (Dirmeyer et al. 2021) uncovered a two-step negative relationship between soil moisture content (*SMC*) and daily air maximum temperature (TA_{max}). When soil moisture content drops below a specific threshold, a stronger negative

relationship has been found. This occurs in a hypersensitive regime below the threshold called the *SMC* breakpoint (*SMbp*), which is found to correspond closely to a property of the vegetation-soil system called the wilting point (WP) (Benson and Dirmeyer 2021). When *SMC* drops below WP, transpiration drops as hydraulic pressure prevents soil water from getting into plant roots (Budyko 1974) and surface evaporation is limited to the meager diffusion of water vapor from the soil matrix into the air, rather than phase changes of liquid water near the surface. Under such conditions, land surface *LE* nearly vanishes and there is no cooling process to offset the various warming processes. The increased amount of compensating *H*, along with intensified upward longwave radiation from hotter surfaces, are hypothesized to become major contributors to the escalation of air temperatures. Accurately estimating the *SMbp* and understanding the physics behind the hypersensitive regime are essential new directions for understanding the mechanism of heatwave and improving forecast skill.

The hypersensitive regime relating *SMC*:TA_{max} that has been diagnosed from observations inherently yields questions: The diagnosed analysis does not directly indicate the casual linkage from land to atmosphere hypothesized above. Are land surface processes indeed responsible for the hypersensitive regime? If so, what are the physical mechanisms inducing feedback in the hypersensitive regime? In this study, we explore these questions using in-situ observations and a simple model for soil evaporation and temperature based on the surface energy-balance relationship.

2. Data and breakpoint analysis

Hourly fields of variables are used from FLUXNET2015 (Pastorello et al. 2020). If land surface processes operate in hypersensitive regimes, theoretically, the same characteristics of sensitivity should be found not only for *SMC*:*TA* relationship but also in the variables involving the chain of energy processing linking land and atmosphere, namely via sensible heat flux (*H*) and surface temperate. As surface radiative temperature, or "skin" temperature, is not measured at these sites, the soil temperature (*TS*) of the topmost soil layer is used as a proxy.

Accordingly, hourly fields of soil moisture content (*SMC*), air temperature (*TA*), soil temperature (*TS*), sensible heat flux (*H*), and latent heat flux (*LE*) are used. We the take shallowest layer *SMC* (typically 5 to 10 cm below the surface) at 0900 local time for analysis to avoid the systematic measurement bias of SMC with diurnal temperature fluctuations (Kapilaratne and Lu 2017). *H* and *LE* are averaged between 0900 and 1200 local time, which is a critical period for land-atmosphere interactions and strongly controlled by *SMC*. Then, breakpoint analysis achieved by piecewise regression (Schwingshackl et al. 2017; Benson and Dirmeyer 2021; Dirmeyer et al. 2021; Hsu and Dirmeyer 2023) is applied to the data from the three warmest calendar months of the recorded period for each site.

At each station and each target month from all available years, one breakpoint is found by piecewise regression. The piecewise regression optimizes the best fit to

minimize the total mean square error across the data space by seeking four parameters: an intersection point (breakpoint values for both *SMC* and its predictand, i.e., *TA, H,* or *TS*), and the slopes for each side of the breakpoint. These four parameters are data-driven without any prejudgment. That is, we do not limit *a priori* the valid range of breakpoints and slopes.

We retain only the results that are considered as a detection of hypersensitive regime by the following screenings: First, the sensitivity of the variable has to match physical understanding — the slope on the both sides of the breakpoint must be negative as soil wetness must negatively affect temperature by land-atmosphere interactions. Second, the dry-side slope must be steeper than the wet-side slope, so it corresponds to a hypersensitive regime. Finally, the difference of the slopes across the breakpoint must pass the significant test at $p<0.05$ level. To obtain statistical significance, degrees of freedom (DOF) are firstly estimated with the sample size divided by $\tau+1$, where τ is the one-day lagged autocorrelations of the SMC timeseries consisting of the daily 0900 LT values of target months catenated across available years. Then, the p-value is obtained by the two sample Z-test using the adjusted DOF. The same test is applied for the significance of the differences in slopes in Figure 3b.

3. Hypersensitive regimes detected from in-situ observations

We take the site CN-Qia (26.7°N,115.°E) as an example to show the hypersensitive characteristics in the *SMC*:TA_{max} relationship (Figure 1a). A *SMbp* separates the *SMC*:TA_{max} as a negative slope on its wet side (black dots fitted by a red line) and a more negative slope on its dry side (brown dots fitted by a gray line). The slope of the fitted regression lines serves as an indicator for the sensitivity. The slope difference across the *SMbp* is statistically significant with $p<0.01$, which validates the detection of *SMbp* and a hypersensitive regime. The same hypersensitive patterns are also seen for *SMC*:*H* and *SMC*:TS_{max} (Figure 1b&c). With $TA_{max,}$ *H, and* TS_{max} respectively representing the land, land-atmosphere interface, and atmosphere links of this land-to-atmosphere process chain, these results imply the hypersensitive regime found in TA_{max} can be attributed to land surface processes. Comparing with the *SMC*:*LE* relationship (Figure 1d; *SMbp* is set as the value of breakpoint for *SMC*:TA_{max}), the patterns hint that the hypersensitive regime happens when there is a drop in *LE* and available energy is mostly channeled into *H* when soils reach a certain dryness.

The same analysis is conducted across other flux sites for the recorded three warmest calendar months throughout all available years of data. Figure 2 shows the available sites from FLUXNET2015. Sites with a colored triangle indicate that the hypersensitive regimes are detected in all three *SMC*:TA_{max}, *SMC*:*H,* and *SMC*:TS_{max} relationships. Hypersensitive regimes are found over 37 out of 267 available sites, which is not a large amount. This may be mainly attributed to the inherent variations across locations in soil type, land cover and climatological background states. FLUXNET2015 is mainly an ecological monitoring network whose tower locations are skewed toward wetter vegetated sites. Across most

sites, soils seldom get dry enough to reach an effective SMbp, no regime transitions are detected.

4. Land surface processes contribute to hypersensitive regimes

A statistical approach as described above raises a doubt: although hypersensitive regimes are found from the land through the atmosphere, it does not necessarily indicate a causal linkage between land and atmosphere. The detected hypersensitive regimes found in these pairs of variables might be determined by chance. We resolve this concern by two analyses: (1) If the hypersensitive regimes are randomly determined, there will be a spread of the *SMbp* determined for $SMC{:}TA_{max}$, $SMC{:}H$, and $SMC{:}TS_{max}$. Accordingly, if they are aligned for three sets of analysis, *SMbp* must be a quantity emerging from physical constraints linking these relationships. (2) If the hypersensitive regimes are induced by land surface processes, the sensitivity of $SMC{:}TS_{max}$ will be stronger than that of $SMC{:}TA_{max}$, based on the second law of thermodynamics. As energy moves from the soil to the atmosphere, a greater portion of it is lost, resulting in a comparatively reduced sensitivity of the hypersensitive regime in the atmosphere compared to that of the soils. That is, the dry-side slope of regression for $SMC{:}TS_{\max}$ should be steeper than that of $SMC{:}TA_{max}$.

Figure 3a displays the difference of the percentile values of the *SMbp* between $SMC{:}TS_{max}$ and $SMC{:}H$ (x-axis) and between $SMC{:}H$ *and* $SMC{:}TA_{max}$ (y-axis) for each site where the hypersensitive regimes are detected in the land-to-atmosphere chain. Chi-square tests are used to estimate the statistical significance of these differences. For all sites, no significant difference is identified, as indicated by the p-value chart (Figure 3b). Thus, the alignment of *SMbp* throughout the land, land-atmosphere interface, and atmosphere supports the argument that *SMbp* emerge from consistent physical processes.

Figure 3c compares the magnitude of sensitivity between $SMC{:}TA_{max}$ and $SMC{:}TS_{max}$ at the dry side of their corresponding *SMbp*. In most sites, sensitivity in $SMC{:}TA_{max}$ is not stronger than in $SMC{:}TS_{max}$ and their difference is statistically significant even though a few sites show different relationships. US-ARb (35.5°N, 98°W) stands out from these cases, presumably related to the fact that the site was burned in March 2005 in the middle of its analyzed period. Its land cover type is identified as barren sparse vegetation, which is also unique among all available sites. Nevertheless, the general pattern here showing a stronger hypersensitive regime in the land than in the atmosphere hints that land surface processes are the driver leading the exacerbated heating of surface air temperature during dry soil conditions — hypersensitive regimes in TA_{max} result from the rapid increase in *H* over extremely dry and warm soils.

5. A toy energy-balance model explains the hypersensitive regimes

The last step to explain the occurrence of the hypersensitive regime is to investigate why the increase in *TS* with drying soils becomes sharper when soil wetness drops below *SMbp.* This would require an energy budget of soils in top few centimeters. However, such an analysis is unable to be executed for most of

in-situ sites where ground heat flux is not measured. We have built a simple physical model based on the surface energy balance equation for a soil layer under different soil dryness conditions in moisture-limited regimes.

Our model explores the hypersensitive regime behavior of SMC:TS_{max} based on the surface energy budget equation. The set of equations to calculate all components are listed below:

$$d(Cs\ TS)/dt = R - LE - H - G \quad (1)$$

$$H = C_h\,(TS - TA) \quad (2)$$

$$G = C_g\,(TS - TG) \quad (3)$$

$$dTS = TS^* - TS \quad (4)$$

R is net radiation, which is set as a constant 1000 W/m^2. H stands for sensible heat flux and G stands for ground heat flux. These two fluxes are described as products of the thermal conductivities (C_h and C_g) and the respective temperature gradients. TS, TA, and TG stand for top layer soil temperature, air temperature, and ground temperature below the surface soil layer, respectively. C_s is soil heat capacity. C_h, C_g, and C_s are tunable parameters (unit: kJ K^{-1} kg^{-1}). They can be set as constants or as functions of SMC; however, either choice does not affect the interpretation of the results and thus is not a focus here. TS^* is the updated state of TS.

WP is set at SMC equal 0.09 m^{3}m^{-3}. LE is determined as a function of SMC and input energy R based on the SMC:LE characteristic in different surface hydrology models described above when SMC>WP. For BM, the linear relationship:

$$LE = R\,(SMC - 0.09) \quad (5)$$

For SWAP, the exponential relationship:

$$LE = R\,(SMC - 0.09)^k \quad (6)$$

where k is a constant and must be set between 0 and 1 to mimic SMC:LE characteristic in SWAP. Here, k is set arbitrarily to 0.5; its precise value does not affect the pattern of TS^*.

The toy model estimates TS by prescribing LE under given initial soil wetness conditions. As a result, the rate of increase in TS is determined by the imbalance

in energy among net radiation (*R*) and heat fluxes at the land surface. With the above set of equations, this toy model assumes that: (1) we perfectly know how *LE* reacts with *SMC* and the rest of the states are modeled after *LE* is determined. (2) Surface layer soil temperature *TS* perfectly represents skin temperature, so *H* is determined by air-soil temperature gradient. (3) Air temperature *TA* and deep layer soil temperature *TG* are constants as they do not respond to available energy as quickly as *TS*. In the default experiment, initial conditions for *TS*, *TA*, and *TG* are set to 293.15K. *Ch, Cg,* and *Cs* are set to 1 kJ K^{-1} kg^{-1}. *TS** in Figure 4 is obtained after one-hour energy input with *SMC* states tested at 0.01 m^3m^{-3} intervals. In the extreme case experiments, *Ch, Cg,* and *Cs* are set with extremely small values (1/10 times default value) or extremely large values (10 times default value).

In this idealized test, we find that precise values of these quantities and parameters are not crucial. The key factor to permit the occurrence of a hypersensitive regime is the functional relationship between *LE* and *SMC.* Two sets of experiments are implemented by setting *LE* as different functions of *SMC* based on two different widely-used hydrologic models: the bucket model (BM) (Manabe 1969; Laio et al. 2001; Porporato et al. 2001) and the Soil Water Atmosphere Plant (SWAP) model (van Dam et al. 2008).

Within the BM framework, evaporation is controlled by saturation deficiency in *SMC*. When *SMC* is insufficient to meet the atmospheric demand, in this model the saturated *SMC,* evaporation decreases linearly from a maximum value at the saturated *SMC* to zero at a value of *SMC* close to WP. Based on this physical moisture behavior, *L*E is described as a simple linear function of *SMC* when *SMC*>WP (cyan line in Figure 4a).

SWAP considers more realistic and thus complex circumstances of soil hydraulic properties. Mainly, the calculation of evapotranspiration takes into account a reduction of root water uptake with soil water depletion and a changing hydraulic conductivity with decreasing soil water. As a result, evapotranspiration decreases nonlinearly from the saturated *SMC* to the WP. Accordingly, the relation of *LE* to *SMC* can be simplified as a power function when *SMC* >WP (cyan line in Figure 4b).

Bold black lines display the responses of *TS* when prescribing an input energy of 1000 W/m^2 after an hour under a default set of parameters describing thermal conductivity for *G* and *H* and soil heat capacity. *TS* responses with parameters set to extremely small and large values are displayed by dashed-black and dotted-black lines, respectively. These experiments with tuned parameters serve as sensitivity tests.

In Figure 4a, the results with *LE* determined by BM show that the hypersensitive regime does not emerge. On the other hand, when *LE* is a power function of *SMC*, hypersensitive regime occurs as *LE* drops dramatically and *SMC* dries toward the WP no matter how the parameters are set. The result indicates that the hypersensitive regime happens because of the exacerbated reduction in *LE*

(which is not characterized by the BM evaporation response curve) accompanied by changes in *H* (orange line) and *G* (brown line). The hypersensitive regime declines after soils dry below the WP.

Examining which function can outperform the linear regression to describe *SMC*:*LE* relationship is not a focus here. In fact, besides the power function, using other functions, e.g., exponential model or polynomial model, that can simulate a nonlinear drop in *LE* with *SMC* as presented by SWAP, also achieve a hypersensitive regime. However, practically, a more complex fitting does not universally outperform linear regression for *SMC*:*LE* relationship in FLUXNET2015 when goodness of fit is penalized by the number of parameters (not shown). Nevertheless, the inadequacy of the simple linear model to simulate a hypersensitive regime arises from its failure to account for the accelerated reduction in LE during soil drying. This justifies that SWAP is more realistic than BM not just statistically, but phenomenologically.

6. Discussion

The *SMC*:TA_{max} hypersensitive regime, characterized by a significant shift in the relationship between declining soil moisture and increasing temperatures, has been revealed by recent observational studies. In this study, we identify similar hypersensitive relationships in *SMC*:*H* and *SMC*:TS_{max} (Figure 1&2), which suggests that the exacerbated sensitivity of TA_{max} to dry soils results from land surface processes. This conjecture is supported by the strong agreement of *SMC* breakpoint (*SMbp*) values among *SMC*:$TA_{max,}$ *SMC*:*H, and SMC*:TS_{max} (Figure 3a), indicating that *SMbp* is not just a quantity randomly determined by statistical analysis. This argument is further reinforced by the finding of a generally stronger sensitivity in *SMC*:TS_{max} than in *SMC*:TA_{max} (Figure 3b), which suggests that the hypersensitive characteristic might originate from the land and be communicated to the near surface atmosphere.

The conundrum of what drives the escalation of *TS* under extremely dry soil conditions is solved using a simple energy-balance model with different parameterizations of the response of *LE* to *SMC* (Figure 4). Based on the in-situ data analysis and model results, we demonstrate the causal connection from declining soil moisture to high air temperatures. We show that the *SMC*:TA_{max} hypersensitive regime is active due to land surface energy processes when soils are drying toward the WP, leading to a dramatic drop of *LE.* The available energy is diverted to *H* and *G,* heating the soil and air more rapidly. The tremendous changes in energy partitioning during the dry down cease when *SMC* is below the *WP*.

Our results suggest that the dominance of *SMC* on *LE* variation is the key to trigger the enhanced feedback between soil moisture and temperature. This is linked by an exacerbated heating of dry soils that leads to a surge in release of *H* and thus a higher daily air temperature maximum. A common linear parameterization of *LE* as a function of *SMC* fails to reflect the observed *TS*

response to extremely dry soils. It means that climate models implementing unrealistic parameterizations might underestimate high temperatures under dry conditions, leading to less reliability in the projection of extremes. Therefore, we advocate that numerical simulations should use a realistic parameterization to represent land surface hydrology and water fluxes, especially when the extreme conditions are the scope of the experiments.

Different *TS* responses yielded by BM and SWAP parameterizations of evaporation (Figure 4) also hint at the importance of phenology on the occurrence of the hypersensitive regime. The nonlinear drop of *LE* with drying soils in Figure 4b, which is represented by the SWAP, is a result of the interactions between plant transpiration and soil water (Romano et al. 2011). This may call for further refinements based on land cover type of each *in situ* site to examine how vegetation type/coverage affects the characteristics of the hypersensitive regime. However, most of these sites are covered by natural vegetation or crops. Rarely are direct measurements of the analyzed variables of this study implemented on bare soils. In FLUXNET2015, land cover types for only for 2 out of 267 sites are classified as BSV (Barren Sparse Vegetation), which could stand as the control group for comparison to the vegetated sites for our analysis. The limited sample size blocks our attempt to systematically separate the results by land cover type. A better understanding of the role of vegetation in hypersensitive regimes requires future in-situ measurements across a variety of land cover types.

Figure 4b parallels the recent finding that the *SMbp* for SMC:TA_{max} is close to *WP* (Benson and Dirmeyer 2021; Dirmeyer et al. 2021). The model results further clarify that the hypersensitive regime does not correspond exactly to the so-called dry soil moisture regime ($SMC<WP$) but begins when *SMC* drops close to the *WP*, i.e., the steepest slope in TA_{max} is slightly above *WP*.

Finally, we emphasize the value of detailed descriptions of the land conditions and physics in numerical simulations for forecasts and future climate projections. Modeling land surface processes involves several soil parameters. We show how *SMC* and *LE* are coupled, and the exact value of *WP* is the most important factor controlling the onset of the hypersensitive regime. When considering the energy balance in soils, *WP* is an important threshold reinforcing abnormally high temperatures. For forecasts, a better representation of *SMbp* accompanied by reliable monitoring of soil conditions helps to better predict the level of the hot extremes. Meanwhile, land use change is one of the main anthropogenic drivers of climate change. Land cover spatial heterogeneity is also among the most significant factors affecting hydrology (Gao et al. 2018; Fan et al. 2021), biology (Atauri and Lucio 2001; Yoshioka et al. 2017), and phenology (Honnay et al. 2003; Zhang et al. 2019), which are all sensitive to extremes. Thus, projections of extremes obtained by better representation of soil physics will address a more confident assessment of climate vulnerability and adaptation.

450

Data availability

FLUXNET2015 dataset are available at:
https://fluxnet.org/data/fluxnet2015-dataset/.

Code availability

The code for generating the results and plots of this study have been deposited in the repository under:
https://github.com/hhsu81819/Hypersensitive-Regime-Analysis

Acknowledgements

This work was supported by National Aeronautics and Space Administration (NASA) grant 80NSSC20K1803 (HH) and 80NSSC21K1801 (PAD). ES was supported by the Korea Meteorological Administration Research and Development program under grant RS-2023-00241809.

Competing Interests Statement

The authors declare no competing interests

References

(1) Alvarez-Castro, M. C.; Faranda, D.; Yiou, P. Atmospheric Dynamics Leading to West European Summer Hot Temperatures Since 1851. *Complexity* **2018**, *2018*, 1–10. https://doi.org/10.1155/2018/2494509.

(2) Atauri, J. A.; de Lucio, J. V. The Role of Landscape Structure in Species Richness Distribution of Birds, Amphibians, Reptiles and Lepidopterans in Mediterranean Landscapes. *Landscape Ecology* **2001**, *16* (2), 147–159. https://doi.org/10.1023/A:1011115921050.

(3) Coumou, D.; Rahmstorf, S. A Decade of Weather Extremes. *Nature Clim Change* **2012**, *2* (7), 491–496. https://doi.org/10.1038/nclimate1452.

(4) Della-Marta, P. M.; Luterbacher, J.; von Weissenfluh, H.; Xoplaki, E.; Brunet, M.; Wanner, H. Summer Heat Waves over Western Europe 1880–2003, Their Relationship to Large-Scale Forcings and Predictability. *Clim Dyn* **2007**, *29* (2–3), 251–275. https://doi.org/10.1007/s00382-007-0233-1.

(5) Dirmeyer, P. A.; Balsamo, G.; Blyth, E. M.; Morrison, R.; Cooper, H. M. Land-Atmosphere Interactions Exacerbated the Drought and Heatwave Over Northern Europe During Summer 2018. *AGU Advances* **2021**, *2* (2). https://doi.org/10.1029/2020AV000283.

(6) Eltahir, E. A. B. A Soil Moisture-Rainfall Feedback Mechanism: 1. Theory and Observations. *Water Resour. Res.* **1998**, *34* (4), 765–776. https://doi.org/10.1029/97WR03499.

(7) Erdenebat, E.; Sato, T. Role of Soil Moisture-Atmosphere Feedback during High Temperature Events in 2002 over Northeast Eurasia. *Prog Earth Planet Sci* **2018**, *5* (1), 37. https://doi.org/10.1186/s40645-018-0195-4.

(8) Fan, P. Y.; Chun, K. P.; Mijic, A.; Tan, M. L.; He, Q.; Yetemen, O. Quantifying Land Use Heterogeneity on Drought Conditions for Mitigation Strategies Development in the Dongjiang River Basin, China. *Ecological Indicators* **2021**, *129*, 107945. https://doi.org/10.1016/j.ecolind.2021.107945.

(9) Founda, D.; Pierros, F.; Katavoutas, G.; Keramitsoglou, I. Observed Trends in Thermal Stress at European Cities with Different

Background Climates. *Atmosphere* **2019**, *10* (8), 436. https://doi.org/10.3390/atmos10080436.

(10) Gao, H.; Sabo, J. L.; Chen, X.; Liu, Z.; Yang, Z.; Ren, Z.; Liu, M. Landscape Heterogeneity and Hydrological Processes: A Review of Landscape-Based Hydrological Models. *Landscape Ecol* **2018**, *33* (9), 1461–1480. https://doi.org/10.1007/s10980-018-0690-4.

(11) Honnay, O.; Piessens, K.; Van Landuyt, W.; Hermy, M.; Gulinck, H. Satellite Based Land Use and Landscape Complexity Indices as Predictors for Regional Plant Species Diversity. *Landscape and Urban Planning* **2003**, *63* (4), 241–250. https://doi.org/10.1016/S0169-2046(02)00194-9.

(12) Horton, D. E.; Johnson, N. C.; Singh, D.; Swain, D. L.; Rajaratnam, B.; Diffenbaugh, N. S. Contribution of Changes in Atmospheric Circulation Patterns to Extreme Temperature Trends. *Nature* **2015**, *522* (7557), 465–469. https://doi.org/10.1038/nature14550.

(13) Hsu, H.; Dirmeyer, P. A. Deconstructing the Soil Moisture-Latent Heat Flux Relationship: The Range of Coupling Regimes Experienced and the Presence of Nonlinearity within the Sensitive Regime. *Journal of Hydrometeorology* **2022**. https://doi.org/10.1175/JHM-D-21-0224.1.

(14) Hsu, H.; Dirmeyer, P. A. Soil Moisture-Evaporation Coupling Shifts into New Gears under Increasing CO2. *Nat Commun* **2023**, *14* (1), 1162. https://doi.org/10.1038/s41467-023-36794-5.

(15) Kapilaratne, R. G. C. J.; Lu, M. Automated General Temperature Correction Method for Dielectric Soil Moisture Sensors. *Journal of Hydrology* **2017**, *551*, 203–216. https://doi.org/10.1016/j.jhydrol.2017.05.050.

(16) Kapilaratne, R. G. C. J.; Lu, M. Automated General Temperature Correction Method for Dielectric Soil Moisture Sensors. *Journal of Hydrology* **2017**, *551*, 203–216. https://doi.org/10.1016/j.jhydrol.2017.05.050.

(17) Kornhuber, K.; Petoukhov, V.; Petri, S.; Rahmstorf, S.; Coumou, D. Evidence for Wave Resonance as a Key Mechanism for Generating High-Amplitude Quasi-Stationary Waves in Boreal Summer. *Clim Dyn* **2017**, *49* (5–6), 1961–1979. https://doi.org/10.1007/s00382-016-3399-6.

(18) Koster, R. D.; Milly, P. C. D. The Interplay between Transpiration and Runoff Formulations in Land Surface Schemes Used with Atmospheric Models. *J. Climate* **1997**, *10* (7), 1578–1591. https://doi.org/10.1175/1520-0442(1997)010<1578:TIBTAR>2.0.CO;2.

(19) Laio, F.; Porporato, A.; Ridolfi, L.; Rodriguez-Iturbe, I. Plants in Water-Controlled Ecosystems: Active Role in Hydrologic Processes and Response to Water Stress. *Advances in Water Resources* **2001**, *24* (7), 707–723. https://doi.org/10.1016/S0309-1708(01)00005-7.

(20) Manabe, S. CLIMATE AND THE OCEAN CIRCULATION [1]: I. THE ATMOSPHERIC CIRCULATION AND THE HYDROLOGY OF THE EARTH'S SURFACE. *Mon. Wea. Rev.* **1969**, *97* (11), 739–774. https://doi.org/10.1175/1520-0493(1969)097<0739:CATOC>2.3.CO;2.

(21) Marotzke, J.; Forster, P. M. Forcing, Feedback and Internal Variability in Global Temperature Trends. *Nature* **2015**, *517* (7536), 565–570. https://doi.org/10.1038/nature14117.

(22) Miralles, D. G.; Teuling, A. J.; van Heerwaarden, C. C.; Vilà-Guerau de Arellano, J. Mega-Heatwave Temperatures Due to Combined Soil Desiccation and Atmospheric Heat Accumulation. *Nature Geosci* **2014**, *7* (5), 345–349. https://doi.org/10.1038/ngeo2141.

(23) Mukherjee, S.; Mishra, A. K.; Zscheischler, J.; Entekhabi, D. Interaction between Dry and Hot Extremes at a Global Scale Using a Cascade Modeling Framework. *Nat Commun* **2023**, *14* (1), 277. https://doi.org/10.1038/s41467-022-35748-7.

(24) Pastorello, G.; Trotta, C.; Canfora, E.; Chu, H.; Christianson, D.; Cheah, Y.-W.; Poindexter, C.; Chen, J.-C.; Elbashandy, A.; Humphrey, M.; Isaac, P.; Polidori, D.; Ribeca, A.; Ingen, C.; Zhang, L.; Amiro, B.; Ammann, C.; Arain, M.; Ardö, J.; Papale, D. The FLUXNET2015 Dataset and the ONEFlux Processing Pipeline for Eddy Covariance Data. *Scientific Data* **2020**, *7*.

(25) Perkins, S. E.; Alexander, L. V.; Nairn, J. R. Increasing Frequency, Intensity and Duration of Observed Global Heatwaves and Warm Spells. *Geophys. Res. Lett.* **2012**, *39* (20), 2012GL053361. https://doi.org/10.1029/2012GL053361.

(26) Perkins, S. E.; Alexander, L. V.; Nairn, J. R. Increasing Frequency, Intensity and Duration of Observed Global Heatwaves and Warm Spells.

Geophys. Res. Lett. **2012**, *39* (20), 2012GL053361. https://doi.org/10.1029/2012GL053361.

(27) Perkins-Kirkpatrick, S. E.; Fischer, E. M.; Angélil, O.; Gibson, P. B. The Influence of Internal Climate Variability on Heatwave Frequency Trends. *Environ. Res. Lett.* **2017**, *12* (4), 044005. https://doi.org/10.1088/1748-9326/aa63fe.

(28) Petoukhov, V.; Rahmstorf, S.; Petri, S.; Schellnhuber, H. J. Quasiresonant Amplification of Planetary Waves and Recent Northern Hemisphere Weather Extremes. *Proc. Natl. Acad. Sci. U.S.A.* **2013**, *110* (14), 5336–5341. https://doi.org/10.1073/pnas.1222000110.

(29) Porporato, A.; Laio, F.; Ridolfi, L.; Rodriguez-Iturbe, I. Plants in Water-Controlled Ecosystems: Active Role in Hydrologic Processes and Response to Water Stress. *Advances in Water Resources* **2001**, *24* (7), 725–744. https://doi.org/10.1016/S0309-1708(01)00006-9.

(30) Romano, N.; Palladino, M.; Chirico, G. B. Parameterization of a Bucket Model for Soil-Vegetation-Atmosphere Modeling under Seasonal Climatic Regimes. *Hydrol. Earth Syst. Sci.* **2011**, *15* (12), 3877–3893. https://doi.org/10.5194/hess-15-3877-2011.

(31) Santanello, J. A.; Dirmeyer, P. A.; Ferguson, C. R.; Findell, K. L.; Tawfik, A. B.; Berg, A.; Ek, M.; Gentine, P.; Guillod, B. P.; van Heerwaarden, C.; Roundy, J.; Wulfmeyer, V. Land–Atmosphere Interactions: The LoCo Perspective. *Bulletin of the American Meteorological Society* **2018**, *99* (6), 1253–1272. https://doi.org/10.1175/BAMS-D-17-0001.1.

(32) Schumacher, D. L.; Keune, J.; Dirmeyer, P.; Miralles, D. G. Drought Self-Propagation in Drylands Due to Land–Atmosphere Feedbacks. *Nat. Geosci.* **2022**, *15* (4), 262–268. https://doi.org/10.1038/s41561-022-00912-7.

(33) Schwingshackl, C.; Hirschi, M.; Seneviratne, S. I. Quantifying Spatiotemporal Variations of Soil Moisture Control on Surface Energy Balance and Near-Surface Air Temperature. *Journal of Climate* **2017**, *30* (18), 7105–7124. https://doi.org/10.1175/JCLI-D-16-0727.1.

(34) Seneviratne, S. I.; Lüthi, D.; Litschi, M.; Schär, C. Land–Atmosphere Coupling and Climate Change in Europe. *Nature* **2006**, *443* (7108), 205–209. https://doi.org/10.1038/nature05095.

(35)

Seo, E.; Lee, M.-I.; Jeong, J.-H.; Koster, R. D.; Schubert, S. D.; Kim, H.-M.; Kim, D.; Kang, H.-S.; Kim, H.-K.; MacLachlan, C.; Scaife, A. A. Impact of Soil Moisture Initialization on Boreal Summer Subseasonal Forecasts: Mid-Latitude Surface Air Temperature and Heat Wave Events. *Clim Dyn* **2019**, *52* (3–4), 1695–1709. https://doi.org/10.1007/s00382-018-4221-4.

(36) Seo, E.; Lee, M.-I.; Schubert, S. D.; Koster, R. D.; Kang, H.-S. Investigation of the 2016 Eurasia Heat Wave as an Event of the Recent Warming. *Environ. Res. Lett.* **2020**, *15* (11), 114018. https://doi.org/10.1088/1748-9326/abbbae.

(37) Sheridan, S. C.; Lee, C. C. Temporal Trends in Absolute and Relative Extreme Temperature Events Across North America. *J. Geophys. Res. Atmos.* **2018**, *123* (21). https://doi.org/10.1029/2018JD029150.

(38) Sutton, R. T.; Hodson, D. L. R. Atlantic Ocean Forcing of North American and European Summer Climate. *Science* **2005**, *309* (5731), 115–118. https://doi.org/10.1126/science.1109496.

(39) van Dam, J. C.; Groenendijk, P.; Hendriks, R. F. A.; Kroes, J. G. Advances of Modeling Water Flow in Variably Saturated Soils with SWAP. *Vadose Zone Journal* **2008**, *7* (2), 640–653. https://doi.org/10.2136/vzj2007.0060.

(40) Vargas Zeppetello, L. R.; Battisti, D. S.; Baker, M. B. The Origin of Soil Moisture Evaporation "Regimes." *Journal of Climate* **2019**, *32* (20), 6939–6960. https://doi.org/10.1175/JCLI-D-19-0209.1.

(41) Vogel, M. M.; Zscheischler, J.; Seneviratne, S. I. Varying Soil Moisture–Atmosphere Feedbacks Explain Divergent Temperature Extremes and Precipitation Projections in Central Europe. *Earth Syst. Dynam.* **2018**, *9* (3), 1107–1125. https://doi.org/10.5194/esd-9-1107-2018.

(42) Wehrli, K.; Guillod, B. P.; Hauser, M.; Leclair, M.; Seneviratne, S. I. Identifying Key Driving Processes of Major Recent Heat Waves. *J. Geophys. Res. Atmos.* **2019**, *124* (22), 11746–11765. https://doi.org/10.1029/2019JD030635.

(43) Whan, K.; Zscheischler, J.; Orth, R.; Shongwe, M.; Rahimi, M.; Asare, E. O.; Seneviratne, S. I. Impact of Soil Moisture on Extreme Maximum Temperatures in Europe. *Weather and Climate Extremes* **2015**, *9*, 57–67. https://doi.org/10.1016/j.wace.2015.05.001.

(44) Yoshioka, A.; Fukasawa, K.; Mishima, Y.; Sasaki, K.; Kadoya, T. Ecological Dissimilarity among Land-Use/Land-Cover Types Improves a Heterogeneity Index for Predicting Biodiversity in Agricultural Landscapes. *Ambio* **2017**, *46* (8), 894–906. https://doi.org/10.1007/s13280-017-0925-7.

(45) Yu, S.; Yan, Z.; Freychet, N.; Li, Z. Trends in Summer Heatwaves in Central Asia from 1917 to 2016: Association with Large-scale Atmospheric Circulation Patterns. *Int J Climatol* **2020**, *40* (1), 115–127. https://doi.org/10.1002/joc.6197.

(46) Zaitchik, B. F.; Macalady, A. K.; Bonneau, L. R.; Smith, R. B. Europe's 2003 Heat Wave: A Satellite View of Impacts and Land–Atmosphere Feedbacks. *Int. J. Climatol.* **2006**, *26* (6), 743–769. https://doi.org/10.1002/joc.1280.

(47) Zander, K. K.; Botzen, W. J. W.; Oppermann, E.; Kjellstrom, T.; Garnett, S. T. Heat Stress Causes Substantial Labour Productivity Loss in Australia. *Nature Clim Change* **2015**, *5* (7), 647–651. https://doi.org/10.1038/nclimate2623.

(48) Zhang, X.; Liu, L.; Henebry, G. M. Impacts of Land Cover and Land Use Change on Long-Term Trend of Land Surface Phenology: A Case Study in Agricultural Ecosystems. *Environ. Res. Lett.* **2019**, *14* (4), 044020. https://doi.org/10.1088/1748-9326/ab04d2.

(49) Benson, D. O.; Dirmeyer, P. A. Characterizing the Relationship between Temperature and Soil Moisture Extremes and Their Role in the Exacerbation of Heat Waves over the Contiguous United States. *Journal of Climate* **2021**, *34* (6), 2175–2187. https://doi.org/10.1175/JCLI-D-20-0440.1.

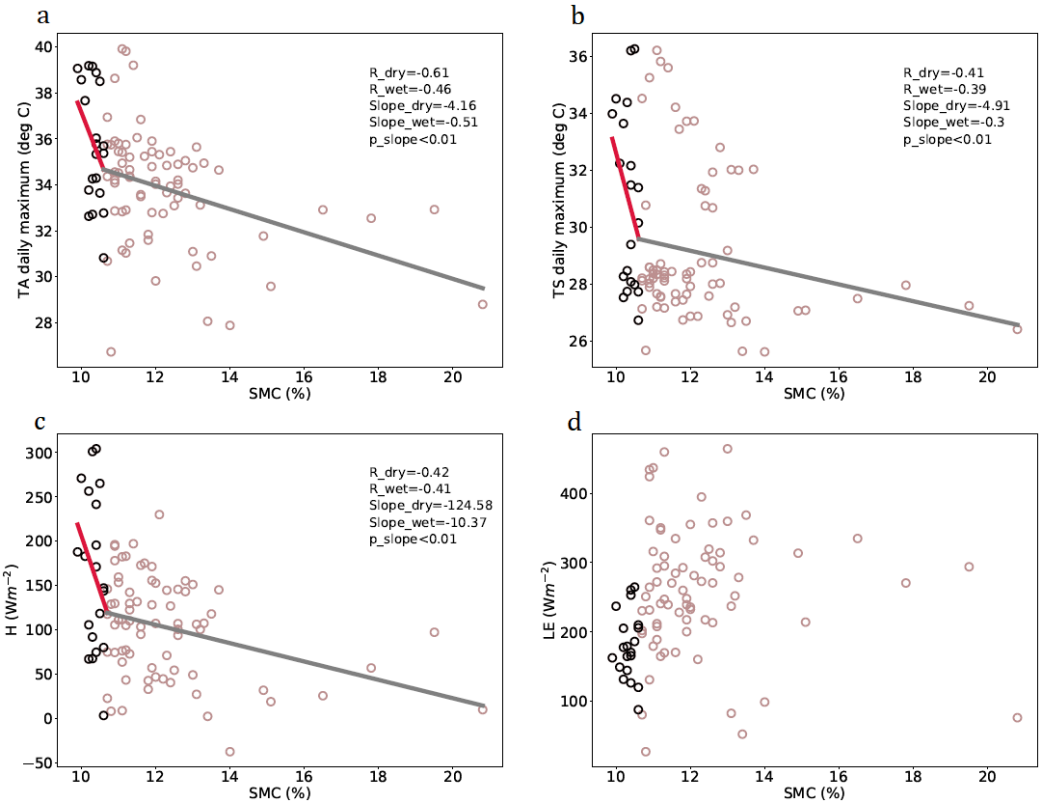

Figure 1| Hypersensitive regime as detected over FLUXNET2015 site CN-Qia (26.7°N,115.°E) during 2003-2005 August. Scatter plot showing the *SMC* breakpoint (*SMbp*) determined by piecewise regression for daily (a) 0900 local time soil moisture content *SMC* and daily air temperature maximum TA_{max}, (b) *SMC* and daily surface layer soil temperature maximum TS_{max}, and (c) *SMC* and 0900-1200 mean sensible heat flux *H*. *SMC* values below *SMbp* are black symbols fitted by the red regression. *SMC* values above *SMbp* are brown symbols fitted by the black regression. R_dry indicates the Pearson correlation between the variables and Slope_dry measures the sensitivity between variables for subsamples on the dry side of *SMbp*; likewise for R_wet and Slope_wet but for subsamples on the wet side of *SMbp*. The p-value for statistical significance of the difference between Slope_dry and Slope_wet is indicated by p_slope, calculated by a two sample Z-test. Scatter plot (d) displays the relationship between *SMC* and 0900-1200 mean latent heat flux *LE*; dot color is determined by its position relative to *SMbp* from the *SMC*:TA_{max} relationship.

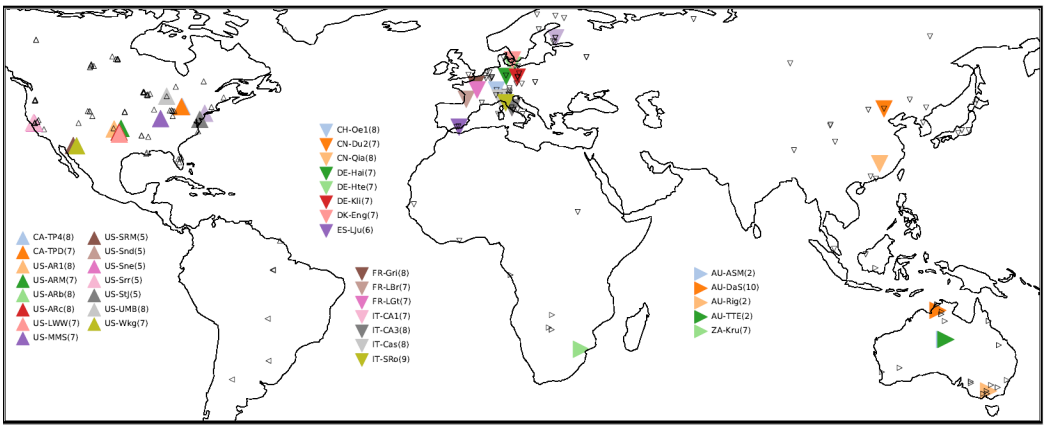

Figure 2| Available sites provided by FLUXNET2015 and the sites where hypersensitive regimes are detected. A total of 267 *in situ* flux tower sites are provided by FLUXNET2015; locations for each are indicated by a triangle. We target the month with the recorded maximum climatological air temperature and its adjacent months for analysis (Note that data may not be available for all months at specific sites). Sites with breakpoints detected for $SMC{:}TA_{\max}$, $SMC{:}TS_{\max}$, and $SMC{:}H$ relationships are colored and noted in the legends. Numbers in the parentheses following the site names indicate the month when the hypersensitive regimes are detected. For any site, hypersensitive regimes may be detected for more than one month. In these cases, we retain the result in the following order: warmest month>its previous month>its next month. The orientation of the triangles distinguishes different geographic regions.

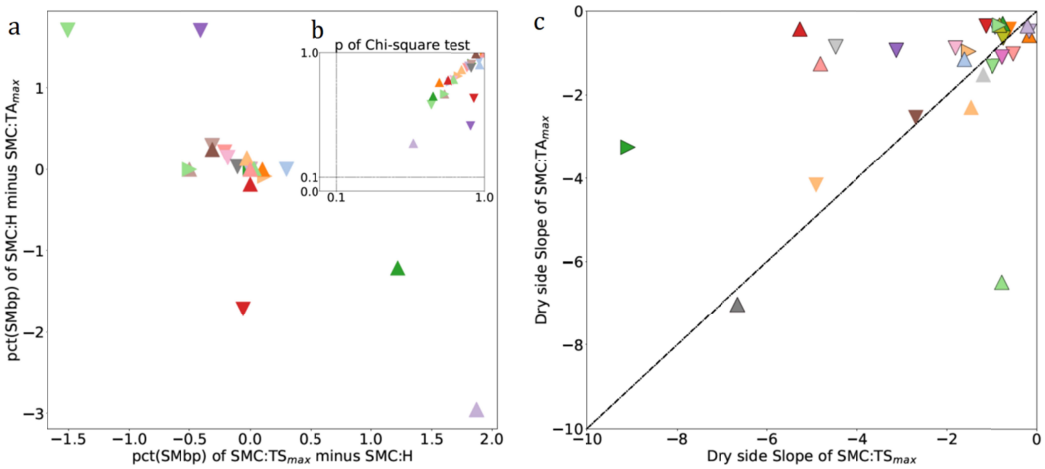

Figure 3| Alignment of breakpoint and sensitivity magnitude for land and atmosphere variables supports the argument of a casual linkage in the hypersensitive regime. The scatter plot (a) displays the difference of the percentiles of the *SMC* breakpoint (SMbp) between *SMC*:TS_{max} and *SMC*:*H* (x-axis) versus the difference of the percentile of SMbp between *SMC*:*H* and *SMC*:TA_{max} (y-axis). The significance of difference is tested by a Chi-square test with null hypothesis that SMbp partitions the same number of samples at its dry side. The p-values of the test for each pair of variables at each site are displayed in the inset (b). Scatter plot (c) displays the dry side slope of *SMC*:TS_{max} (x-axis) and *SMC*:TA_{max} (y-axis); if the difference is statistically significant with $p<0.05$ by a two sample Z-test, the symbol is outlined in black.

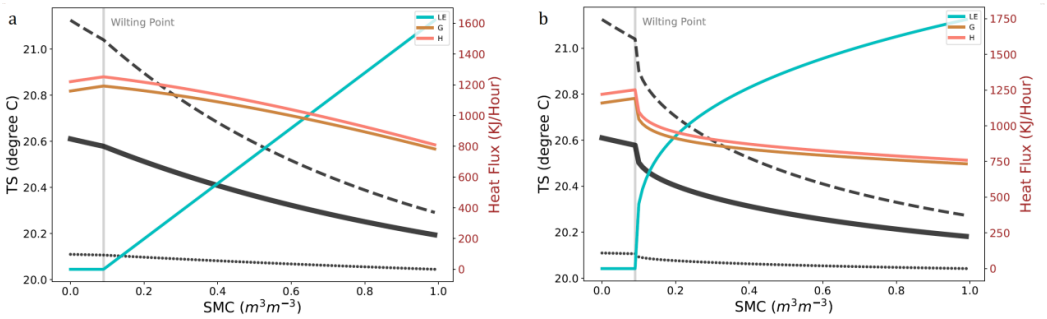

Figure 4| Responses of soil temperatures and heat fluxes yielded by the toy energy-balance model. The toy model explores how soil temperature *TS* will evolve at different values of soil moisture content *SMC* after an hour of 1000 W/m^2 energy input in response to the budget of latent heat flux *LE*, sensible heat flux *H*, and ground heat flux *G*. In case (a) *LE* is prescribed based on the bucket model parameterization: *LE* linearly increases with wetting soils when it is above the wilting point. In case (b) *LE* is prescribed by a power function of *SMC*: *LE* nonlinearly increases with wetter soils when it is above a wilting point, in better agreement with observations. *TS* as a function of *SMC* with parameters for soil physics set as reasonable values, extremely small and extremely large values are shown by the bold black lines, dashed lines and dotted lines, respectively. The two extreme lines enclose a range of heating responses in *TS* in soils with different physical characteristics.